SCIENTIA PLENA
www.scientiaplena.org.br
VOL. 22, NUM. 03 2026
doi: 10.14808/sci.plena.2026.034201

Use of rice husk ash as an adsorbent in the removal of tartrazine yellow and methylene blue from aqueous solutions: A kinetic and thermodynamic study

Uso da cinza da casca de arroz como adsorvente na remoção de amarelo de tartrazina e azul de metileno de soluções aquosas: Um estudo cinético e termodinâmico

F. A. C. Biasuz[1]; N. S. Leite[1]; O. B. Garla[1]; J. G. da S. de Andrade[2*]; S. L. F. Rosa[3]; F. R. de Carvalho[1]

[1]*Department of Technology, State University of Maringa, 87506-370, Umuarama-PR, Brazil*
[2]*Postgraduate Program in Chemical Engineering, State University of Maringa, 87020-900, Maringa-PR, Brazil*
[3]*Department of Mechanical Engineering, State University of Maringa, 87020-900, Maringa-PR, Brazil*

**joaogabriel-andrade@hotmail.com*
(Recebido em 27 de abril de 2025; aceito em 02 de março de 2026)

Rice husk ash (RHA) is an abundant byproduct of the food industry. While frequently used as a fertilizer, this application can lead to the polluting accumulation of residual carbon in the soil. Research suggests that RHA can serve as a cost-effective alternative adsorbent to high-cost activated carbon. In this study, RHA was chemically treated with NaOH (RHA-b) and H_3PO_4 (RHA-a) to enhance the adsorption of the anionic dye tartrazine yellow (TY) and the cationic dye methylene blue (MB). Structural analysis identified silanol groups and a slit-like pore morphology on the RHA surface.Kinetic studies revealed that equilibrium was reached faster for MB (180 minutes) than for TY (240 minutes), with experimental data best described by the pseudo-second-order kinetic model. RHA-b exhibited the highest removal efficiency, reaching 93% for MB and 54% for TY. Regarding isothermal studies, the Langmuir model provided the best fit for the experimental data. The maximum adsorption capacities were determined to be 20.21 and 19.92 mg g^{-1} for MB (RHA-a and RHA-b, respectively) and 3.29 and 9.29 mg g^{-1} for TY (RHA-a and RHA-b, respectively). Thermodynamic parameters indicated that adsorption was a spontaneous process for all adsorbents, with the highest spontaneity observed for MB adsorption on RHA ΔG^{o}_{ads} = -34.5 kJ mol^{-1}. Furthermore, spontaneity was driven by enthalpy in TY adsorption and by entropy in MB adsorption.
Keywords: adsorption, rice husk ash, thermodynamics.

A cinza de casca de arroz (RHA) é um subproduto abundante da indústria alimentícia. Embora comumente utilizada como fertilizante, essa aplicação pode causar o acúmulo poluente de carbono residual no solo. Estudos indicam que a RHA pode atuar como adsorvente alternativo ao carvão ativado de alto custo. Neste trabalho, a RHA foi tratada quimicamente com NaOH (RHA-b) e H_3PO_4 (RHA-a) para otimizar a adsorção do corante aniônico amarelo tartrazina (TY) e do catiônico azul de metileno (MB). Estruturalmente, identificaram-se grupos silanol e morfologia de poros do tipo fenda na superfície da RHA.
Os estudos cinéticos revelaram que o equilíbrio foi alcançado em 180 minutos para o MB e 240 minutos para o TY, com os dados experimentais sendo melhor descritos pelo modelo de pseudo-segunda ordem. A RHA-b apresentou a maior eficiência de remoção, atingindo 93% para MB e 54% para TY. Nos estudos isotérmicos, o modelo de Langmuir demonstrou o melhor ajuste aos dados. As capacidades máximas de adsorção obtidas foram de 20,21 e 19,92 mg g^{-1} para MB (RHA-a e RHA-b, respectivamente) e de 3,29 e 9,29 mg g^{-1} para TY (RHA-a e RHA-b, respectivamente). Os parâmetros termodinâmicos indicaram que a adsorção foi um processo espontâneo para todos os adsorventes, com maior espontaneidade registrada na adsorção de MB em RHA ΔG^{o}_{ads} = -34,5 kJ mol^{-1}. Além disso, observou-se que a espontaneidade foi impulsionada pela entalpia na adsorção de TY e pela entropia na adsorção de MB.
Palavras-chave: adsorção, cinza da casca de arroz, termodinâmica.

1. INTRODUCTION

The rise in the world population has contributed to the expansion of industrial activities. Satisfactorily, this expansion has supplied the population with food, medicine, clothing, etc. However, a greater number of effluents, with different types of contaminants, have been generated. As many of these contaminants are resistant to chemical, photochemical, and

biological degradation, they are considered extremely harmful to the environment and, hence, to humans [1, 2]. Considering that less than 1% of the planet's water is available for consumption, the lack of adequate treatment and incorrect disposal of these effluents in natural waters is a serious problem [3].

One of the most harmful contaminants in liquid effluents is dyes, which originate from the textile, pharmaceutical, food, and various other industrial sectors [4]. The presence of dyes or pigments in industrial effluents is because they are not completely consumed during the production process. It is estimated that there are more than 10 thousand types of dyes generated by the different types of existing industries, generating approximately 800 thousand tons of dyes annually [5, 6]. The presence of dyes in rivers, resulting from inadequate disposal, tends to reduce the water's reoxygenation capacity, the passage of sunlight, and photosynthetic activity [7, 8]. Among the dyes, the class of azo dyes and phenothiazines is the most used by industries [9], such as tartrazine yellow (TY) and methylene blue (MB), respectively.

TY is an anionic dye (Figure 1A) and one of the most commonly used dyes in the coloring of pharmaceuticals, beverages, and foods. Nevertheless, TY is regarded as toxic due to its potential to cause allergic reactions, migraines, eczema, thyroid cancer, hives, and lupus. Even though TY toxicity, it is permitted in many countries, such as Brazil, Canada, the United States, and the European Union, and is one of the most utilized food colorings in the world [10, 11]. MB is a cationic dye (Figure 1B) and has been widely applied to color silk, wool, cotton, and paper [12, 13]. MB is not biodegradable and, depending on the dose ingested, it can be carcinogenic. In fact, MB is a threat to human health and can cause serious damage to the environment [14, 15]. Regarding human health, MB can cause respiratory difficulties, abdominal disorders, blindness, digestive problems, and mental disorders [16, 17].

In this context, methods for removing dyes are extremely important for preserving the environment and human well-being. Several traditional methods result in other pollutants as secondary products, causing losses [18]. Therefore, much research has been performed to discover ecological and sustainable methods for removing dyes from natural waters, such as precipitation, chemical degradation, biodegradation, electrocoagulation, chemical coagulation, and adsorption. In particular, adsorption offers significant advantages over other methods, including its low cost, simplicity, and remarkable efficiency in dye removal [19, 20]. Activated carbon is one of the best materials used as an adsorbent to be used to remove dyes from water bodies by adsorption. Nevertheless, the high cost has prompted extensive research into alternative adsorbent materials. Some examples of these adsorbent materials are bamboo waste [21], coconut shell [22], sugar cane bagasse [23], almond shell [24], orange peel [25], banana peel [26], rice husk [27], and others [28, 29].

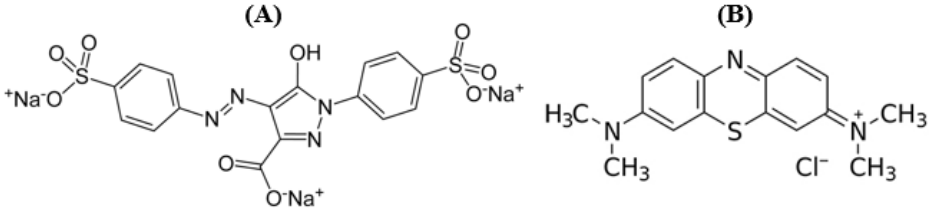

Figure 1: Chemical structures of tartrazine yellow (TY) (A) and methylene blue (MB) (B).

In the food industry, rice husk (RH) is one of the most significant by-products generated. To add value to this abundant biomass, industries have increasingly utilized rice husks as an alternative energy source to fossil fuels, particularly in boilers for steam generation. However, the direct combustion of rice husks generates ash that, if improperly disposed of, can lead to environmental pollution, as residual carbon in large quantities poses a significant threat to soil quality [30, 31]. In pursuit of a more sustainable disposal method for rice husk ash (RHA), researchers have observed compelling results regarding its potential as a highly effective adsorbent for dyes in natural water bodies. Lakshmi et al. (2009) [32] studied the adsorption of the dye indigo carmine and obtained an adsorption capacity between 29.3 and 65.9 mg g^{-1},

depending on the temperature. Razak et al. (2013) [33] investigated the removal of methylene blue and found a removal of 96.1%. In this same study, the authors found that RHA was more effective in adsorbing the dye than RH. Khan et al. (2022) [34] chemically modified RHA and achieved 99.1% removal of the crystal violet dye at pH 6, using a dosage of 2.0 g L^{-1} of adsorbent. RHA was also used to adsorb the dye brilliant green [35], congo red [36], acid orange 7 [37], malachite green [38], remazol red [39], and reactive orange 16 [40].

This study seeks to rigorously investigate and critically compare the adsorption processes of the TY/RHA and MB/RHA systems, which have not yet been reported in the literature. The RHA was characterized in its raw form (RHA-r), treated in an acidic medium (RHA-a), and treated in a basic medium (RHA-b). The kinetics and adsorption study were performed, and the thermodynamic parameters were determined for all systems.

2. MATERIALS AND METHODS

2.1 Chemical treatment of RHA

The RHA was collected at Zaeli Food Industry, located in the city of Umuarama, Paraná State, Brazil. RHA was used in three forms: (i) raw (RHA-r), (ii) treated in acid medium-H_3PO_4 (RHA-a), and (iii) treated in basic medium-NaOH (RHA-b). Firstly, the RHA was left to rest in contact with distilled water for 24 h to remove water-soluble species. After, the mixture was filtered. Then, the RHA was dried in the oven for 2 h at 105 °C and sieved, seeking homogeneity in particle size. For the acid and base treatment, the sieved RHA was placed in contact with a solution of H_3PO_4 (0.1 mol L^{-1}) or NaOH (0.1 mol L^{-1}), under stirring for 24 h. After carrying out the acid or basic treatment, the RHA was filtered, washed with distilled water several times to remove the acid or basic residue, and dried again in the oven for 2 h at 105 °C.

2.2 Characterization of RHA

The RHA ATR-FTIR spectra were obtained with an ATR-FTIR spectrophotometer (Agilent Cary, 630), using a platinum module and diamond crystal for attenuated total reflection, from 400 to 4000 cm^{-1}. The X-ray diffractograms (XRD) were collected with a Shimadzu XRD6000 X-ray diffractometer using Ni-filtered Cu-K α radiation (λ = 0.154 nm) at 40 kV and 30 mA, with a diffraction angle (2Θ) ranging from 10 to 60°. The crystallinity index (CrI) was determined by Eq. 1 (Segal et al., 1959) [41]:

$$\mathbf{CrI} = \left(\frac{\mathbf{Intensity_c - Intensity_{am}}}{\mathbf{Intensity_c}}\right)\mathbf{x100} \qquad \text{Eq. 1}$$

where $Intensity_c$ is approximately the crystalline cellulose content, and $Intensity_{am}$ is approximately the amorphous cellulose content.

The scanning electron microscopy (SEM) images were obtained with a QUANTA 250 FEI microscope with an operating accelerating voltage of 12.50 kV. The samples were metallized with gold, and the images were magnified at 800x.

The surface area, volume, and size of pores and the distribution of pores in the adsorbent were determined using gas (N_2) adsorption analysis. Internal structure analysis is primarily concerned with the structure of adsorbent pores. The area surface and pore diameters of the adsorbents were measured using data from the adsorption-desorption process. The models developed by Brunauer, Emmett, and Teller (BET) and Barrett, Joyner, and Halenda (BJH), describe the phenomenon of adsorption, to determine the volume of adsorbed gas as a function of relative pressure. To determine the micropore volume, the t-plot method was applied.

The point of zero charge (pH_{PZC}) assesses the surface charge of adsorbents. It was estimated by adding 0.100 g of each adsorbent to 100 mL of a 1.00 mol L^{-1} KCl solution and 100 mL of

distilled water. The experiments were performed in duplicate. After stirring for 15 min, the samples were centrifuged, and the *pH* values were measured using a *pH* meter (Quimis, Q-400MT). Employing Eq. 2 and 3, the Δ*pH* and pH_{PZC}, respectively, were determined (Batistela et al., 2016) [42]:

$$\Delta pH = pH_{KCl} - pH_{H_2O} \quad \text{Eq. 2}$$

$$pH_{PZC} = 2\,x\,pH_{KCl} - pH_{H_2O} \quad \text{Eq. 3}$$

where pH_{KCl} is the *pH* in KCl solution, pH_{H2O} is the *pH* in water, Δ*pH* is the difference between pH_{KCl} and pH_{H2O}, and *pHpcz* is the *pH* where the adsorbent surface is neutral.

2.3 Adsorptions kinetics Study

The initial concentration of the TY and MB solution was 20 mg L^{-1} [43, 44]. From these solutions, an aliquot of 10.0 mL was collected and introduced into Falcon tubes. A fixed dosage of 10.0 g L^{-1} was used for each adsorbent (RHA-r, RHA-a, and RHA-b). The RHA was introduced into the TY or MB solution to ensure complete immersion, with a controlled *pH* of 2 [43] for the TY/RHA system and 11 [44] for the MB/RHA system. The tubes were closed and mechanically agitated in a shaker. After each time interval, the adsorbent was removed, and the concentrations of free TY and MB in the solution were quantified using a UV-Vis spectrophotometer. The experiment was performed in triplicate. The amount of TY and MB adsorbed (Q_t) was calculated according to Eq. 4:

$$\boldsymbol{Q_t = \left(\frac{Ci - Cf}{m_{adsorbent}}\right) x V_{solution}} \quad \text{Eq. 4}$$

where Q_t is the amount of TY or MB adsorbed by the adsorbent at each time *t* (mg g^{-1}), C_i is the initial concentration of the dye solution (mg L^{-1}), C_f is the final concentration of the dye solution (mg L^{-1}), $V_{solution}$ is the volume of the adsorbate solution (L), and $m_{adsorbent}$ is the mass of adsorbent used (g). The kinetic studies were performed in triplicate, and the mathematical models applied were pseudo-first order (PPO) and pseudo-second order (PSO).

2.4 Adsorptions isotherms Study

The isothermal study was conducted by fixing the equilibrium time determined in the kinetic study and applying different initial concentrations of the adsorbate (TY and MB). This study was also performed for the three forms of RHA (RHA-r, RHA-a, and RHA-b), with the dosage fixed at 12.0 g L^{-1}. A total of 10.0 mL of the TY or MB solution was added at a specified initial concentration, along with 0.012 g of adsorbent in Falcon tubes. The *pH* was maintained at 2 for the TY/RHA system and at 11 for the MB/RHA system. The tubes were closed and mechanically agitated in a shaker. After the shaking period, an aliquot of the solution was removed, and the absorbance was measured using a UV-Vis spectrophotometer. The experiment was performed in triplicate. The adsorbent capacity was calculated according to Eq. 4, and the adsorption parameters were determined using the mathematical models of Langmuir and Freundlich, represented by Eq.5 and 6, respectively:

$$q_e = \left(\frac{q_m K_L C_e}{1 + K_L C_e}\right) \quad \text{Eq. 5}$$

$$q_e = K_F C_e^{\frac{1}{n}} \quad \text{Eq. 6}$$

where q_e is the equilibrium adsorption capacity (mg g^{-1}), q_m is the maximum adsorption capacity (mg g^{-1}), C_e is the equilibrium concentration (mg L^{-1}), K_L is the Langmuir constant (L mg^{-1}), K_F is the Freundlich constant, and n is the constant that indicates the adsorption intensity.

2.5 Thermodynamic parameters

To determine the thermodynamic parameters (ΔH^o_{ads}, ΔS^o_{ads}, and ΔG^o_{ads}), adsorption isotherms were investigated at various temperatures (25, 35, and 45 °C). At each temperature, the experimental procedure outlined in section 2.3 was followed. The mathematical model employed was the Langmuir model. Since the Langmuir constant (K_L) is not dimensionless, a correction factor was required for its proper application in the equation $\Delta G^o_{ads} = -RT\ln K^o$ [45]. Therefore, Eq. 7 was applied as a correction factor:

$$K^o = K_L \, x \, M_{adsorbate} \, x \, 10^3 \, x \, 55.5 \qquad \text{Eq. 7}$$

where K^o is the thermodynamic equilibrium constant (dimensionless), and $M_{adsorbate}$ is the molar mass of the adsorbate (g mol^{-1}). Employing the K^o values obtained at each temperature, the van't Hoff equation (Eq. 8) was applied to determine the values of the standard enthalpy of adsorption (ΔH^o_{ads}) and the standard entropy of adsorption (ΔS^o_{ads}):

$$\ln K^o = \frac{\Delta S^o_{ads}}{R} - \frac{\Delta H^o_{ads}}{RT} \qquad \text{Eq. 8}$$

where R is the ideal gas constant (8.314 J mol^{-1} K^{-1}), and T is the temperature in Kelvin (K). The values of ΔH^o_{ads} and ΔS^o_{ads} were determined by plotting $\ln K^o$ versus $1/T$. The variation of the standard Gibbs free energy of adsorption (ΔG^o_{ads}) of adsorption was determined by applying Eq. 9.

$$\Delta G^o_{ads} = -RT\ln K^o \qquad \text{Eq. 9}$$

3. RESULTS AND DISCUSSION

3.1 Characterization of rice husk ash

3.1.1 ATR-FTIR spectra and X-ray diffraction patterns

Rice husk ash (RHA) results from the combustion of rice husks, which likely causes the decomposition of much of the organic matter in the agro-industrial residue, such as hemicellulose, cellulose, and lignin. The ATR-FTIR spectra confirm this decomposition by showing the absence of some of the characteristic signals from these compounds. According to Yang et al. (2007) [46], hemicellulose is the first to decompose within a temperature range of 220 to 315 °C. Cellulose then begins to decompose between 315 and 400 °C. Finally, lignin, which is the most resistant to decomposition, decomposes more slowly from room temperature up to 900 °C. The ATR-FTIR spectra of RHA under different conditions (RHA-r, RHA-a, and RHA-b) were obtained and are presented in Figure 2A.

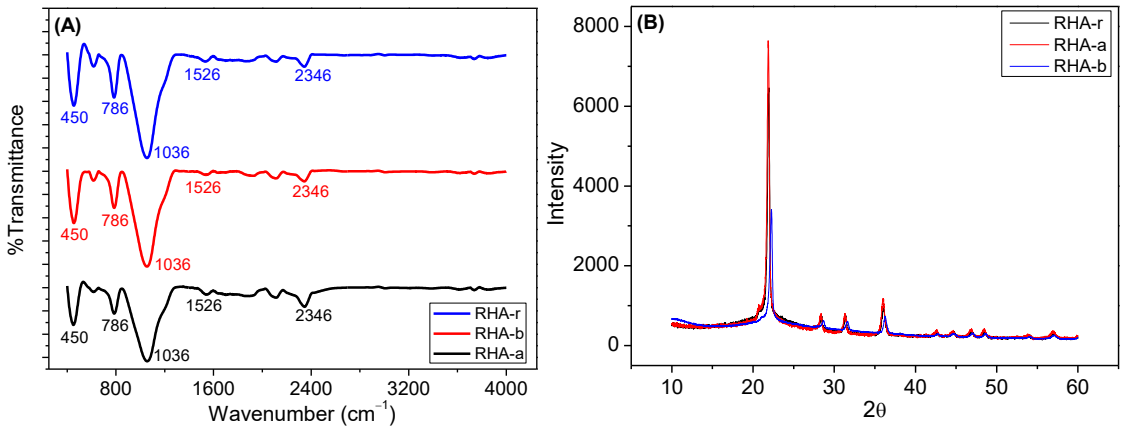

Figure 2: ATR-FTIR spectra (A) and X-ray diffraction patterns (B) for RHA-r, RHA-a, and RHA-b.

The ATR-FTIR spectra (Figure 2A) show similar peaks across the three conditions analyzed, suggesting that the composition and structure of RHA-r, RHA-a, and RHA-b are comparable. Silica signals appear in the spectra of all three conditions, as the combustion of rice husks generally produces a concentration of amorphous silica, typically exceeding 90% [47-50]. The signals observed around 450, 786, and 1036 cm^{-1} correspond to Si-O bonds [51]. The signal at 1036 cm^{-1} is indicative of C-O bonds, which indicates cellulose content related to the C-O bond in cellulose [52]. This result indicates that cellulose was not completely decomposed. A more intense signal is observed in the RHA-r condition, where cellulose remained unaffected by acid hydrolysis [53] or basic hydrolysis [54]. In contrast, under basic conditions (RHA-b), lignin undergoes primary degradation [55]. The small peak at 1526 cm^{-1} corresponds to C-C stretching in the aromatic ring of lignin. RHA-b shows the smallest peak due to the degradation of lignin under basic conditions [55]. Lastly, the peak at 2346 cm^{-1} is associated with C-H vibration and C-O stretching in polysaccharides [56].

Figure 2B shows four well-defined peaks between 21° and 36°. The observed peaks are likely associated with silica, since a significant amount of organic matter decomposes during the rice husk combustion process. This result supports the silica signal observed in the FTIR analysis (Figure 2A). The sharpness of these peaks (Figure 2B) suggests the presence of crystalline silica, specifically an allotropic form of silica named cristobalite [50]. The crystallinity index can be observed in Table 1.

Table 1. Crystallinity index of the adsorbents: RHA-r, RHA-a, and RHA-b.

Parameters	RHA-r	RHA-a	RHA-b
I_c	6379	7547	3319
I_{am}	525	547	509
Crystallinity index	92%	93%	85%

Table 1 shows that all adsorbents exhibited a relatively high crystallinity index. The lowest crystallinity index was observed for RHA-b, likely due to the NaOH attack on crystalline silica [57].

3.2.2 Scanning electron microscopy (SEM)

The RHA samples were analyzed employing SEM to obtain essential information on the surface characteristics of the materials, which can significantly influence the adsorption process. The images of the adsorbents, magnified at 800x, are presented in Figure 3.

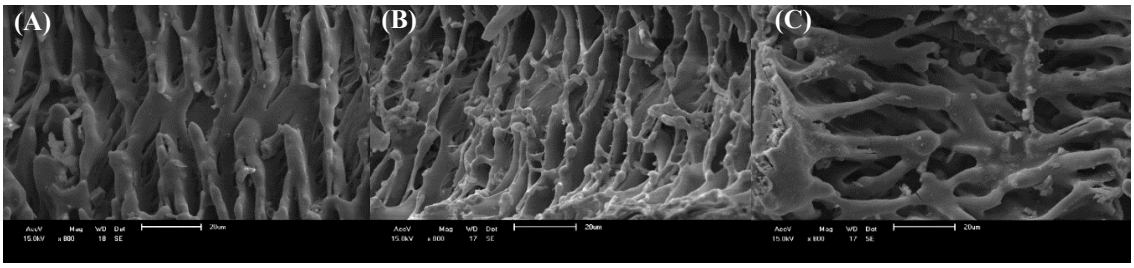

Figure 3: SEM images of the adsorbents: RHA-r (A), RHA-a (B), and RHA-b (C).

Figure 3 displays that the three samples (A: RHA-r, B: RHA-a, and C: RHA-b) exhibit a similar heterogeneous and slit-like pore morphology on the surface. In addition, all images reveal an irregular network of elongated voids and interconnected channels, which is characteristic of silica-rich agricultural residues.

3.2.3 Surface area assessment: BET, BJH, and t-plot methods

The surface area of the adsorbents was determined by applying the Brunauer-Emmett-Teller (BET) method. The total pore volume was calculated by the Barrett-Joyner-Halenda (BJH) desorption method, and the micropore volume was determined by the t-plot method [58]. The results are presented in Table 2.

Table 2: Surface area, total pore volume, micropore volume, and average pore diameter for RHA under different conditions.

Condition	Surface area ($m^2\ g^{-1}$)	Total pore volume ($cm^3\ g^{-1}$)	Micropore volume ($cm^3\ g^{-1}$)	Average pore diameter (Å)
RHA-r	36.58	0.01664	0.00965	37.34
RHA-a	45.35	0.01522	0.01010	39.94
RHA-b	46.16	0.01757	0.00854	37.52

A surface area of 45.35 $m^2\ g^{-1}$ for RHA-a and 46.16 $m^2\ g^{-1}$ for RHA-b was obtained (Table 2). These values are higher than those of RHA-r (36.58 $m^2\ g^{-1}$), which is consistent with the findings reported in the literature [59]. Although the chemical treatment produced an increase in surface area, this change is modest, and the differences among the samples may fall within the experimental uncertainty typically associated with BET measurements. The average pore diameter (Table 2) classifies the pores as mesopores [58]. The shape of the isotherms presented in Figure 4 is characteristic of multilayer adsorption and resembles a type II isotherm, indicating both multilayer adsorption and the presence of micropores. The hysteresis observed in the isotherms of Figure 4 indicates the presence of non-rigid agglomerates with plate-like particles, which generate slit-shaped pores [58]. This result is consistent with the SEM images (Figure 3), which also show slit-shaped pores.

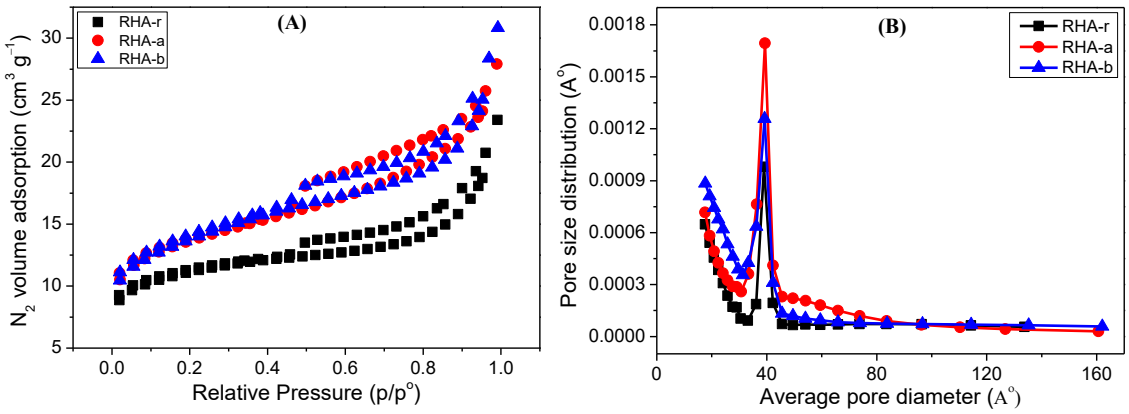

Figure 4: BET isotherms (A) and pore size distribution as a function of average pore diameter (B) for RHA-r, RHA-a, and RHA-b.

3.2.4 Determination of point of zero charge (pH_{PZC})

The pH_{PZC} (Table 3) represents the *pH* at which the adsorbent surface is electrically neutral. This value is crucial for assessing the electrostatic interactions between the adsorbent and adsorbate. When $pH_{solution} < pH_{PZC}$, the adsorbent surface carries a positive charge on its surface. Conversely, when the $pH_{solution} > pH_{PCZ}$, the adsorbent surface carries a negative charge on its surface [60, 61]. At $pH_{solution}$ 2.0, the optimal $pH_{solution}$ for TY dye [43], all RHA conditions show a positive surface charge, promoting the adsorption of TY (an anionic dye). In contrast, at $pH_{solution}$ 11, the optimal $pH_{solution}$ for MB [44], all RHA conditions display a negative surface charge, promoting the adsorption of MB (a cationic dye).

Table 3: pH_{PZC} values for the adsorbents studied at 25.0 °C.

Adsorbents	pH_{KCl}	pH_{H2O}	ΔpH	pH_{PZC}
RHA-r	7.30±0.10	8.51±0.03	–1.21±0.13	6.10±0.23
RHA-a	5.57±0.03	6.36±0.07	0.79±0.10	4.79±0.13
RHA-b	6.47±0.03	7.16±0.11	0.69±0.13	5.78±0.16

Table 3 demonstrates that, under all experimental conditions, the pH_{PZC} values fall within the acidic *pH* range, with the most acidic value observed for RHA-a (4.79). Based on the observed pH_{PZC} values, electrostatic attractions favor the adsorption of both TY and MB dyes for all adsorbents.

3.2 Adsorptions kinetics Study

The kinetic studies were conducted in triplicate. As illustrated in Figure 5, the adsorption equilibrium was achieved after approximately 240 min for TY and 180 min for MB. This difference in the adsorption time suggests a difference in the adsorption mechanism. The experimental data were best described by the pseudo-second-order kinetic (PSO) model, as illustrated in Figure 5 and in Table 4.

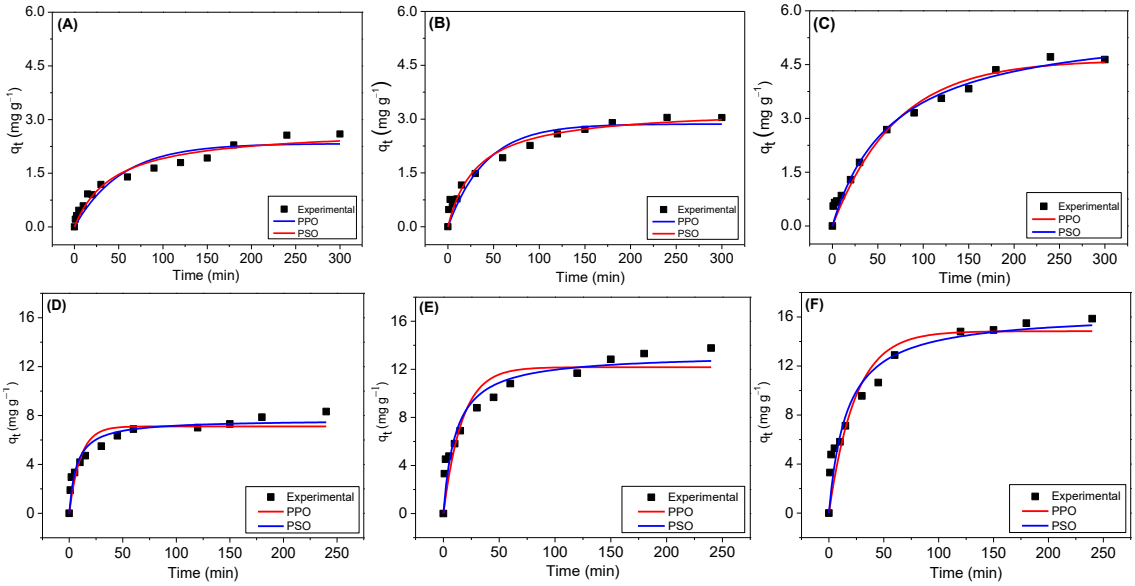

Figure 5: Adsorption kinetics for TY and MB on RHA in different conditions at 25.0 °C. Adsorbent dosage of 10.0 g L^{-1}, pH = 2.0 for TY solution and pH = 11 for MB solution. [TY] = 20.0 mg L^{-1}, [MB] = 10.0 mg L^{-1}. (A) TY/RHA-r; (B) TY/RHA-a; (C) TY/RHA-b; (D) MB/RHA-r; (E) MB/RHA-a and (F) MB/RHA-b.

Table 4: Kinetic parameters for TY and MB adsorption on RHA in different conditions at 25.0 °C. Dosage = 10.0 g L^{-1}, pH = 2.0 for TY adsorption and pH = 11 for MB adsorption. [TAR] = 20.0 mg L^{-1} and [MB] = 10.0 mg L^{-1}.

Models	**PPO**			**PSO**		
Systems	q_e **(mg g^{-1})**	k_1 **(min^{-1})**	**R²**	q_e **(mg g^{-1})**	k_2 **(g mg^{-1} min^{-1})**	**R²**
TY/RHA-r	2.33±0.14	0.019±0.004	0.9218	2.76±0.17	0.008±0.003	0.9570
TY/RHA-a	2.86±0.14	0.024±0.005	0.9293	3.30±0.18	0.010±0.002	0.9569
TY/RHA-b	4.63±0.21	0.014±0.002	0.9723	5.75±0.32	0.003±0.001	0.9808
MB/RHA-r	7.11±0.38	0.097±0.023	0.8640	7.68±0.33	0.019±0.005	0.9356
MB/RHA-a	12.18±0.73	0.060±0.015	0.8544	13.28±0.72	0.007±0.002	0.9193
MB/RHA-b	14.84±0.85	0.042±0.009	0.8899	16.36±0.93	0.004±0.001	0.9119

The PSO model provided the best fit for the experimental values. This model assumes that chemisorption may be the phase controlling the adsorption rate, where the valence forces, resulting from the sharing or exchange of electrons between the adsorbent and the adsorbate, are considered [62]. Phihusut and Chantharat (2017) [63] compared the adsorption efficiency of MB on RH and RHA. The values of q_e and k_2 obtained in this study were consistent with those reported by the authors under similar experimental conditions.

The observed q_e values (Table 4) demonstrate that RHA adsorbs more MB dye compared to TY, indicating a stronger affinity of RHA for cationic dyes. The chemically treated adsorbents exhibited superior efficiency in adsorbing both dyes, particularly for MB. These results suggest that the increased surface roughness and porosity of the adsorbents (evident in Figures 3B, 3C, and Table 2), as a result of chemical treatment, contribute to the enhancement of dye removal from aqueous solutions. The kinetic data further allowed for the assessment of the removal efficiency for each system, as illustrated in Figure 6. For both dyes, the highest removal efficiencies were observed for RHA treated in a basic medium (RHA-b), achieving 93% and 54% for the MB/RHA-b and TY/RHA-b systems, respectively.

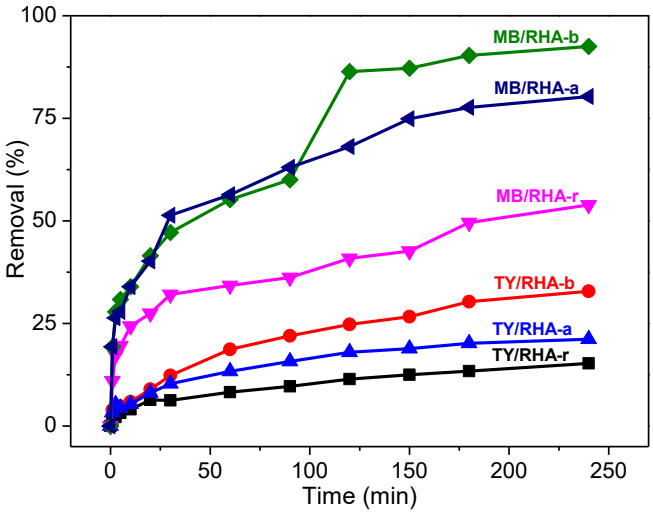

Figure 6: Percentage of MB and TY removal using RHA under different conditions at 25.0 °C. Adsorbent dosage of 10.0 g L^{-1}, pH = 2.0 for TY solution and pH = 11 for MB solution. [TY] = 20.0 mg L^{-1}, [MB] = 10.0 mg L^{-1}.

The principal component of RHA is silica, as observed in the ATR-FTIR spectra (Figure 2A). This implies that its surface contains silanol groups, such as $(SiO)_3{-}SiOH$ and $(SiO)_2{-}Si{-}(OH)_2$ [64]. These groups exhibit pK_a values of 4.5 and 8.5, respectively [65]. The chemical treatment with NaOH caused the deprotonation of the silanol OH groups, thereby making the negative charges on the surface of the material more intense. The MB adsorption was conducted at *pH* 11, ensuring that the adsorbent surface remained deprotonated throughout the process. Thus, the negative charge on the surface of the material originates from residual negative charges, since $pH > pH_{PZC}$, and from negative charges of deprotonated chemical groups.

In the adsorption of TY, the solution *pH* (*pH* = 2) plays a decisive role because, under highly acidic conditions, the silanol groups on the RHA surface become protonated. Since $pH < pH_{PZC}$, the surface acquires a net positive charge, which favors the adsorption of the anionic dye through electrostatic attraction. Accordingly, a higher adsorption capacity would normally be expected for RHA-a, as the acidic treatment favors the protonation of surface sites. However, the experimental results showed the opposite trend. As presented in Figure 6, TY removal reached 21% for RHA-a and 33% for RHA-b, despite the fact that the alkaline-treated sample does not present a stronger electrostatic attraction toward the dye. Because the BET surface areas of RHA-a and RHA-b are very similar (45.35 and 46.16 $m^2\ g^{-1}$, respectively; Table 2), and the differences fall within the expected experimental uncertainty of the technique, surface area variations cannot explain the observed adsorption behavior. These findings indicate that TY adsorption onto RHA is influenced by factors beyond surface charge. The distinct chemical treatments likely generated subtle but relevant differences in surface chemistry and microstructure, such as modifications in functional groups, surface roughness, pore accessibility, and the amount or nature of residual carbon. Even when not reflected in significant changes in total surface area, these effects can alter diffusion, affinity, and interaction strength between the adsorbent surface and the dye molecules [66]. A similar result was reported by Bertolani et al. (2024) [67], who observed that, for tartrazine adsorption onto pigeon pea husk, structural and chemical changes introduced by the treatment processes exerted a more significant influence on adsorption performance than surface area alone. In this context, the higher adsorption of TY onto RHA-b suggests that the chemical and microstructural modifications induced by alkaline treatment played a more dominant role in the adsorption mechanism than surface charge effects.

The removal of MB from aqueous solutions is significantly higher compared to the removal of TY. This fact is probably related to the strong electrostatic interactions between the negatively charged surface of RHA and the cationic MB molecules. A similar behavior was verified by Hongo et al. (2021) [68], who reported a removal efficiency exceeding 80% for MB at *pH* 11, employing RHA from a power plant in Myanmar, a country in South Asia.

3.3 Adsorptions isotherm Study

The isotherm studies were carried out by fixing the equilibrium time found in the kinetic study (240 min for TY and 180 min for MB) at different initial concentrations of the adsorbate. The experimental data were best represented by the Langmuir model, as shown in Figure 7 and in the R^2 values presented in Table 4. This model suggests that the adsorption process of TY and MB on the surface of RHA, under all conditions, was chemical adsorption (chemisorption), homogeneous, and monolayer. Furthermore, it indicates that the adsorption process occurs at specific sites [69].

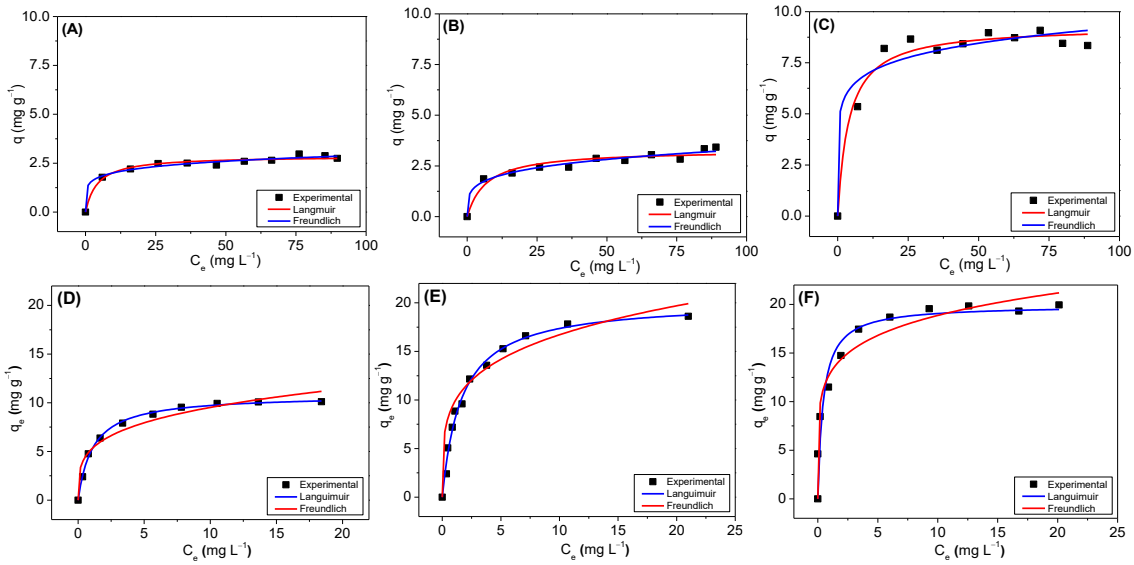

Figure 7: Adsorption isotherm for TY and MB on RHA in different conditions at 25.0 °C. Adsorbent dosage of 10.0 g L^{-1}, pH = 2.0 for TY solution and pH = 11 for MB solution. (A) TY/RHA-r; (B) TY/RHA-a; (C) TY/RHA-b; (D) MB/RHA-r; (E) MB/RHA-a and (F) MB/RHA-b.

The evaluation of the maximum adsorption capacity values (q_m) for the TY/RHA system shows that TY adsorption was higher on RHA-b, reaching q_m = 9.29 mg g^{-1}, as presented in Table 4. This result is consistent with the TY removal percentages observed in Figure 6, confirming that the superior performance of RHA-b cannot be attributed to surface area differences, which are negligible. Instead, the result supports the interpretation that chemical and microstructural changes induced by the alkaline treatment exert a more significant influence on the adsorption behavior than surface charge effects alone. Evaluating the q_m of the MB/RHA system, it can be seen that under conditions where RHA was chemically treated, the values were higher, 20.21 mg g^{-1} and 19.92 mg g^{-1} for RHA-a and RHA-b, respectively, as shown in Table 5. This result is consistent with the MB removal percentage observed in Figure 6. However, in this case, both chemically treated adsorbents had a higher adsorption capacity, not just RHA-b, as seen in the TY/RHA-b system. Salem et al. (2018) [70] found a similar result when studying the adsorption of MB on untreated and HCl- and NaOH-treated RHA. The authors found the value of 28.42 mg g^{-1} for MB adsorption on NaOH-treated RHA, 15.64 mg g^{-1} for MB adsorption on HCl-treated RHA, and 17.36 mg g^{-1} for MB adsorption on untreated RHA [70]. This is an interesting result because it suggests that dye adsorption on the surface of adsorbents should consider not only van der Waals forces and electrostatic interactions, but also the chemical structure of the adsorbate [71]. In fact, the kinetic data demonstrated different equilibrium times for each dye, probably due to differences in the structure of the dye molecules (charge and spatial geometry).

Table 5: Adsorption parameters for TY and MB adsorption on RHA in different conditions at 25.0 °C. Dosage = 10.0 g L^{-1}, pH = 2.0 for TY adsorption and pH = 11 for MB adsorption. [TAR] = 20.0 mg L^{-1} and [MB] = 10.0 mg L^{-1}.

Models	Langmuir			Freundlich		
Systems	q_m (mg g^{-1})	K_L (L mg^{-1})	R^2	K_F ($mg^{1-1/n}$ $L^{1/n}$ g^{-1})	n	R^2
TY/RHA-r	2.87±0.08	0.24±0.05	0.9733	1.39±0.11	6.24±0.80	0.9812
TY/RHA-a	3.29±0.17	0.15±0.05	0.9296	1.15±0.13	4.37±0.54	0.9723
TY/RHA-b	9.29±0.27	0.25±0.06	0.9699	5.19±0.76	8.00±2.45	0.9256
MB/RHA-r	10.81±0.13	0.89±0.05	0.9972	5.21±0.40	3.82±0.51	0.9487
MB/RHA-a	20.21±0.51	0.61±0.05	0.9905	9.69±0.22	4.22±0.17	0.9239
MB/RHA-b	19.92±0.99	2.23±0.78	0.9205	12.87±0.95	6.01±1.19	0.9244

Comparing the adsorption of TY and MB on RHA (without chemical treatment), the q_m values obtained were 2.87 mg g^{-1} and 10.81 mg g^{-1} for TY/RHA and MB/RHA, respectively, as shown in Table 4. This result aligns with the removal percentages observed in Figure 6, where 33% and 93% were observed for TY and MB, respectively. Because the MB molecule is flatter than the TY molecule, MB molecules can interact more closely with the adsorbent surface, leading to greater adsorption. Thus, the effects of surface charge, π–π interactions, and hydrogen bonding [71] are expected to be more pronounced for the MB/RHA system than for the TY/RHA system.

3.4 Thermodynamic Study

The adsorption isotherms were performed at three temperatures: 25 ºC, 35 ºC, and 45 ºC. Based on the values of the Langmuir constant (K_L) at different temperatures, Eq. 5 was applied, and subsequently the van't Hoff model (ln(K^o) versus 1/T), as illustrated in Figure 8.

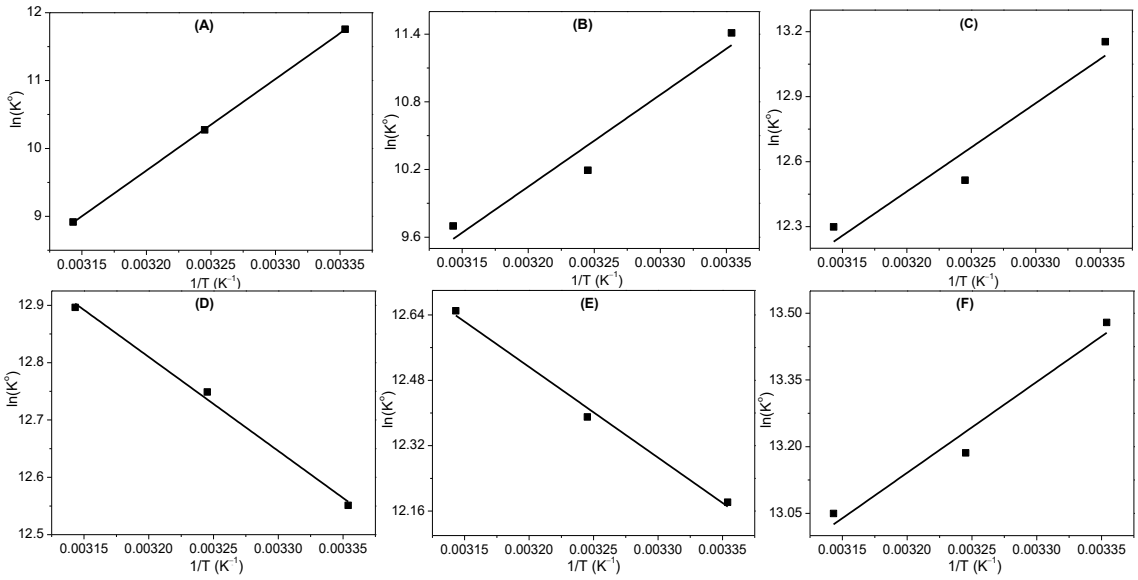

Figure 8: van't Hoff model (ln(K^o) versus 1/T) to determine ΔH^o_{ads} and ΔS^o_{ads} for the systems (A) TY/RHA-r, (B) TY/RHA-a, (C) TY/RHA-b, (D) MB/RHA-r, (E) MB/RHA-a, (F) MB/RHA-b.

Through the slope and intercept, obtained from the above graphs and Eq. 6, the standard adsorption enthalpy (ΔH^o_{ads}) and the standard adsorption entropy (ΔS^o_{ads}) were determined, respectively. The standard adsorption free energy (ΔG^o_{ads}) was calculated by Eq. 7. The thermodynamic parameters are presented in Table 6.

Table 6: Thermodynamic parameters for the adsorption of TY and MB on RHA under different conditions. Dosage = 10.0 g L^{-1}, pH = 2.0 for TY adsorption and pH = 11 for MB adsorption. [TAR] = 20.0 mg L^{-1} and [MB] = 10.0 mg L^{-1}.

Systems	ΔH^o_{ads} (kJ mol^{-1})	ΔS^o_{ads} (J mol^{-1} K^{-1})	ΔG^o_{ads} (kJ mol^{-1})		
			298.15	308.15	318.15
TY/RHA-r	–112.1	–278.1	–29.1	–26.3	–23.6
TY/RHA-a	–67.8	–133.3	–28.3	–26.1	–25.6
TY/RHA-b	–33.9	–4.9	–32.6	–32.0	–32.5
MB/RHA-r	+13.6	+150.1	–31.1	–32.7	–34.1
MB/RHA-a	+18.4	+163.1	–30.2	–31.7	–33.5
MB/RHA-b	–17.0	+54.9	–33.4	–33.8	–34.5

The thermodynamic parameters above revealed that the adsorption of TY and MB onto the RHA surface, under all conditions, is a spontaneous process, with ΔG^o_{ads} ranging from –34.5 to –23.6 kJ mol^{-1}. For the TY/RHA system, the spontaneity is dominated by the standard enthalpy of adsorption (ΔH^o_{ads}). In contrast, for the MB/RHA system, the spontaneity is primarily driven by the standard entropy of adsorption (ΔS^o_{ads}) - except in the case of the MB/RHA-b system, where both the enthalpic (ΔH^o_{ads} = –17.0 kJ mol^{-1}) and entropic (ΔS^o_{ads} = +54.9 J mol^{-1} K^{-1}) contributions are thermodynamically favorable. The MB/RHA system exhibited a higher degree of spontaneity than the TY/RHA system, suggesting stronger interactions between MB molecules and the RHA surface. Both TY and MB showed more spontaneous adsorption under the condition where RHA was treated in a basic medium (RHA-b).

TY adsorption onto RHA occurs via an exothermic process, in contrast to MB adsorption, which is generally endothermic. This indicates that, overall, increasing the temperature tends to favor the adsorption of MB, while it generally disfavors the adsorption of TY onto RHA under most conditions. De Araújo et al. (2021) [71] reported similar findings in their study of TY and MB adsorption onto brewer's spent grain (BSG). They observed a standard adsorption enthalpy of –13.19 kJ mol^{-1} (exothermic process) for TY adsorption on BSG and +40.86 kJ mol^{-1} (endothermic process) for MB adsorption on BSG. However, unlike the results reported by De Araújo et al. (2021) [71], in the present study, TY interacts with RHA predominantly via chemisorption, whereas MB interacts predominantly via physisorption. According to the literature, standard adsorption enthalpy values greater than 40 kJ mol^{-1} (in absolute terms) typically indicate chemisorption, while values lower than 25 kJ mol^{-1} (in absolute terms) are indicative of physisorption [72]. The contrast observed between this study and the findings of De Araújo et al. (2021) [71] highlights that the nature of the adsorbent, and consequently its surface properties, can significantly influence the adsorption mechanism.

The negative values of standard adsorption entropy for the TY/RHA system indicate molecular ordering at the solid–liquid interface during the adsorption process. On the other hand, the positive standard adsorption entropy values for the MB/RHA system suggest molecular disorder at the solid–liquid interface during adsorption.

4. CONCLUSIONS

In this study, the effectiveness of TY and MB adsorption onto RHA under different conditions was investigated: raw form (RHA-r), treated with H_3PO_4 (RHA-a), and treated with NaOH (RHA-b). The characterization of the adsorbents revealed the presence of both crystalline and amorphous silica across all conditions. The surface of the RHA displayed a porous structure characterized by a slit-like morphology. The point of zero charge (pH_{PZC}) of all adsorbents was found in the acidic region, which favored the adsorption of both TY and MB. Adsorption equilibrium was achieved more rapidly in the MB/RHA system (180 min) than in the TY/RHA system (240 min). For the kinetic studies, the experimental data were best described by the pseudo-second-order kinetic model. Among the adsorbents, RHA-b demonstrated the highest dye removal efficiency, achieving 93% of removal for MB and 54% of removal for TY. For the

isotherm studies, the experimental data were best represented by the Langmuir model. The chemically treated adsorbents showed the highest adsorption capacities, reaching 20.21 and 19.92 mg g^{-1} for MB (RHA-a and RHA-b, respectively) and 3.29 and 9.29 mg g^{-1} for TY (RHA-a and RHA-b, respectively). The Thermodynamic parameters demonstrated that the adsorption process was spontaneous in all cases, with greater spontaneity observed in the MB/RHA system, reaching $\Delta G^{o}_{ads} = -34.5$ kJ mol^{-1}. Furthermore, spontaneity was driven by the standard enthalpy of adsorption for the TY/RHA system and by the standard entropy of adsorption for the MB/RHA system. Notably, the MB/RHA-b system was both enthalpically and entropically favorable. Then, RHA-b (NaOH-treated RHA) was identified as the most efficient adsorbent for removing dyes from aqueous solutions, particularly for positively charged dyes such as MB. Finally, these findings underscore the potential of chemically modified RHA as an effective, low-cost, and sustainable adsorbent for wastewater treatment applications.

5. ACKNOWLEDGMENTS

Capes, CNPq and Fundação Araucária.

6. REFERENCES

1. Sharma J, Sharma S, Soni V. Classification and impact of synthetic textile dyes on aquatic flora: a review. Reg Stud Mar Sci. 2021 Jun;45:101802. doi: 10.1016/j.rsma.2021.101802
2. Verma RK, Sankhla MS, Rathod NV, Sonone SS, Parihar K, Singh GK. Eradication of fatal textile industrial dyes by wastewater treatment. Biol Res Appl Chem. 2021 Apr;12(1):567-87. doi: 10.33263/BRIAC121.567587
3. Tkaczyk A, Mitrowska K, Posyniak A. Synthetic organic dyes as contaminants of the aquatic environment and their implications for ecosystems: a review. Sci Total Environ. 2020 May;717:137222. doi: 10.1016/j.scitotenv.2020.137222
4. Maheshwari K, Agrawal M, Gupta AB. Dye pollution in water and wastewater. In: Novel materials, dyes and wastewater treatment. Singapore: Springer; 2021. p. 1-25. doi: 10.1007/978-981-16-2892-4_1
5. Crini G. Non-conventional low-cost adsorbents for dye removal: a review. Bioresour Technol 2006 Jun;97(9):1061-85. doi: 10.1016/j.biortech.2005.05.001
6. Wang MX, Zhang QL, Yao SJ. A novel biosorbent formed of marine-derived *Penicillium janthinellum* mycelial pellets for removing dyes from dye-containing wastewater. Chem Eng J. 2015;259:837-44. doi: 10.1016/j.cej.2014.08.003
7. Daneshvar N, Khataee AR, Ghadim AA, Rasoulifard MH. Decolorization of CI Acid Yellow 23 solution by electrocoagulation process: investigation of operational parameters and evaluation of specific electrical energy consumption (SEEC). J Hazard Mater. 2007 Sep;148(3):566-72. doi: 10.1016/j.jhazmat.2007.03.028
8. Mall ID, Srivastava VC, Agarwal NK. Removal of Orange-G and Methyl Violet dyes by adsorption onto bagasse fly ash — kinetic study and equilibrium isotherm analyses. Dyes Pigm. 2006 May;69(3):210-23. doi: 10.1016/j.dyepig.2005.03.013
9. Hashemi SH, Kaykhaii M. Azo dyes: sources, occurrence, toxicity, sampling, analysis, and their removal methods. In: Emerging freshwater pollution: Analysis, fate and regulation. 4th ed. Amsterdam: Elsevier Academic Press; 2022. p.267-87. doi: 10.1016/B978-0-12-822850-0.00013-2
10. Mittal A, Mittal J, Kurup L. Adsorption isotherms, kinetics and column operations for the removal of hazardous dye, Tartrazine, from aqueous solutions using waste materials – Bottom Ash and De-Oiled Soya as adsorbents. J Hazard Mater. 2006 Aug;136(3):567-78. doi: 10.1016/j.jhazmat.2005.12.037
11. . Leulescu M, Rotaru A, Pălărie I, Moanţă A, Cioateră N, Popescu M, et al. Tartrazine: physical, thermal and biophysical properties of the most widely employed synthetic yellow food-colouring azo dye. J Therm Anal Calorim. 2018 Aug;134:209-31. doi: 10.1007/s10973-018-7663-3
12. Derakhshan Z, Baghapour MA, Ranjbar M, Faramarzian M. Adsorption of Methylene Blue dye from aqueous solutions by modified pumice stone: kinetics and equilibrium studies. Health Scope. 2013 Nov;2(3):136-44. doi: 10.17795/jhealthscope-12492
13. Han TH, Khan MM, Kalathil S, Lee J, Cho MH. Simultaneous enhancement of methylene blue degradation and power generation in a microbial fuel cell by gold nanoparticles. Ind Eng Chem Res. 2013 May;52(24):8174-81. doi: 10.1021/ie4006244

14. Sun L, Hu D, Zhang Z, Deng X. Oxidative degradation of methylene blue via PDS-based advanced oxidation process using natural pyrite. Int J Environ Res Public Health. 2019 Nov;16(23):4773. doi: 10.3390/ijerph16234773
15. Contreras M, Grande-Tovar CD, Vallejo W, Chaves-López C. Bio-removal of methylene blue from aqueous solution by *Galactomyces geotrichum* KL20A. Water. 2019 Feb;11(2):282. doi: 10.3390/w11020282
16. Abdelrahman EA, Hegazey RM, El-Azabawy RE. Efficient removal of methylene blue dye from aqueous media using Fe/Si, Cr/Si, Ni/Si, and Zn/Si amorphous novel adsorbents. J Mater Res Technol. 2019 Nov;8(6):5301-13. doi: 10.1016/j.jmrt.2019.08.051
17. Santoso E, Ediati R, Kusumawati Y, Bahruji H, Sulistiono DO, Prasetyoko D. Review on recent advances of carbon based adsorbent for methylene blue removal from wastewater. Mater Today Chem. 2020 Jun;16:100233. doi: 10.1016/j.mtchem.2019.100233
18. Mohammed FM, Roberts EPL, Hill A, Campen AK, Brown NW. Continuous water treatment by adsorption and electrochemical regeneration. Water Res. 2011 May;45(10):3065-74. doi: 10.1016/j.watres.2011.03.023
19. Wang S, Boyjoo Y, Choueib A, Zhu ZH. Removal of dyes from an aqueous solution using fly ash and red mud. Water Res. 2005 Jan;39(1):129-38. doi: 10.1016/j.watres.2004.09.011
20. Kandisa RV, Saibaba KN, Shaik KB, Gopinath R. Dye removal by adsorption: a review. J Biodivers Bioprospect. 2016 Oct;7(6):377. doi: 10.4172/2155-6199.1000371
21. Wang L. Application of activated carbon derived from 'waste' bamboo culms for the adsorption of azo disperse dye: kinetic, equilibrium and thermodynamic studies. J Environ Manag. 2012 Jul;102:79-87. doi: 10.1016/j.jenvman.2012.02.019
22. Iriarte-Velasco U, Álvarez-Uriarte JI, Chimeno-Alanis N, González-Velasco JR. Natural organic matter adsorption onto granular activated carbons: implications in the molecular weight and disinfection by-products formation. Ind Eng Chem Res. 2008 Sep;47(20):7868-76. doi: 10.1021/ie800912y
23. Al-Mokhalelati K, Al-Bakri I, Al Shibeh Al Wattar N. Adsorption of methylene blue onto sugarcane bagasse-based adsorbent materials. J Phys Org Chem. 2021 Feb;34(7):e4193. doi: 10.1002/poc.4193
24. Omri A, Lambert SD, Geens J, Bennour F, Benzina M. Synthesis, surface characterization and photocatalytic activity of TiO_2 supported on almond shell activated carbon. J Mater Sci Technol. 2014 Sep;30(9):894-902. doi: 10.1016/j.jmst.2014.04.007
25. Harnal VS, Darla U, Lataye DH. Removal of Congo red dye from wastewater using orange peel as an adsorbent. J Indian Assoc. Environ Manage. 2020;40(2):52-9. doi: 10.56042/jiaem.v40i2.37674
26. Akter M, Rahman FBA, Abedin MZ, Kabir SF. Adsorption characteristics of banana peel in the removal of dyes from textile effluent. Textiles. 2021 Sep;1(2):361-75. doi: 10.3390/textiles1020018
27. Nandiyanto ABD, Nugraha WC, Yustia I, Ragadhita R, Fiandini M, Saleh M, et al. Rice husk for adsorbing dyes in wastewater: literature review of agricultural waste adsorbent, preparation of rice husk particles, particle size on adsorption characteristics with mechanism and adsorption isotherm. Adv Res Appl Mech. 2023 Jun;106(1):1-13. doi: 10.37934/aram.106.1.113
28. Mo J, Yang Q, Zhang N, Zhang W, Zheng Y, Zhang Z. A review on agro-industrial waste (AIW) derived adsorbents for water and wastewater treatment. J Environ Manag. 2018 Dec;227:395-405. doi: 10.1016/j.jenvman.2018.08.069
29. Micheletti DH, da Silva AJG, Porto CE, Alves BHM, de Carvalho FR, Sakai OA, et al. A review of adsorbents for removal of yellow tartrazine dye from water and wastewater. Bioresour Technol Rep. 2023 Dec;24:101598. doi: 10.1016/j.biteb.2023.101598
30. Pandey VC, Singh N. Impact of fly ash incorporation in soil systems. Agric. Ecosyst. Environ. 2010 Feb;136(1-2):16-27. doi: 10.1016/j.agee.2009.11.013
31. Panda RB, Biswal T. Impact of fly ash on soil properties and productivity. Int. J Agric Environ Biotechnol. 2018 Jul;11(2):275-83. doi: 10.30954/0974-1712.04.2018.8
32. Lakshmi UR, Srivastava VC, Mall ID, Lataye DH. Removal of dyes using fly ash and agricultural wastes. J Environ Manag. 2009 Feb;90(2):710-20. doi: 10.1016/j.jenvman.2008.01.002
33. Razak NH, Hazmi FA, Tahrim AA. Comparative adsorption studies using low-cost adsorbents of rice husk and rice husk ash on methylene blue dye removal. J Eng Tech. 2013 Dec;4(2):39-48.
34. Khan A, Malik A, Humayun M, Shah N, Ismail M, Yahia M, et al. Improvement of the adsorption efficiency of rice husk ash for crystal violet dye removal from aqueous medium. Egypt. J Chem. 2022 Nov;65(131):427-35. doi: 10.21608/EJCHEM.2022.122775.5496
35. Mane VS, Mall ID, Srivastava VC. Kinetic and equilibrium isotherm studies for the adsorptive removal of Brilliant Green dye from aqueous solution by rice husk ash. J Environ Manag. 2007 Sep;84(4):390-400. doi: 10.1016/j.jenvman.2006.06.024

36. Chowdhury AK, Sarkar AD, Bandyopadhyay A. Rice husk ash as a low-cost adsorbent for the removal of methylene blue and Congo red in aqueous phases. Clean–Soil, Air, Water. 2009 Jul;37(7):581-91. doi: 10.1002/clen.200900051
37. Barbosa TR, Foletto EL, Dotto GL, Jahn SL. Preparation of mesoporous geopolymer using metakaolin and rice husk ash as synthesis precursors and its use as potential adsorbent to remove organic dye from aqueous solutions. Ceram Int. 2018 Jan;44(1):416-23. doi: 10.1016/j.ceramint.2017.09.193
38. Banerjee S, Debsarkar A, Datta S. Adsorption of two basic dyes methylene blue and malachite green onto low-cost adsorbent rice husk ash: a batch study. Int J Agric Environ Biotechnol. 2018 Sep;11(3):421-6. doi: 10.30954/0974-1712.06.2018.1
39. Costa JAS, Paranhos CM. Evaluation of rice husk ash in adsorption of Remazol Red dye from aqueous media. Sci Appl Sci. 2019 Apr;1:397. doi: 10.1007/s42452-019-0436-1
40. Akbar Ali AM, Karthikeyan RK, Sentamil SM, Mithilesh KR, Madhangi P, Maheswari N, et al. Removal of Reactive Orange 16 by adsorption onto activated carbon prepared from rice husk ash: statistical modelling and adsorption kinetics. Sep Sci Technol. 2020 Dec;55(1):26-34. doi: 10.1080/01496395.2018.1559856
41. Segal LGJM, Creely JJ, Martin AE Jr, Conrad CM. An empirical method for estimating the degree of crystallinity of native cellulose using X-ray diffractometer. Text Res J. 1959 Oct;29(10):786-94. doi: 10.1177/004051755902901003
42. Batistela VR, Fogaça LZ, Fávaro SL, Caetano W, Fernandes-Machado NRC, Hioka N. ZnO supported on zeolites: photocatalyst design, microporosity, and properties. Colloids Surf. A Physicochem. Eng. Aspects. 2016 Nov;513:20-7. doi: 10.1016/j.colsurfa.2016.11.02
43. Santos LN, Porto CE, Bulla MK, Batistela VR, Barros BCB. Peach palm and cassava wastes as biosorbents of tartrazine yellow dye and their application in industrial effluent. Sci. Plena. 2021 May;17(5):1-19. doi: 10.14808/sci.plena.2021.054201
44. Da Silva AJG, Porto CE, Moreira WM, Batistela VR, Scaliante MHNO. Production of hydrochars from *Pinus caribaea* for biosorption of methylene blue and tartrazine yellow dyes. Clean Chem Eng. 2023 Mar;5:100092. doi: 10.1016/j.clce.2022.100092
45. Zhou X, Zhou X. The unit problem in the thermodynamic calculation of adsorption using the Langmuir equation. Chem Eng Commun. 2014 Nov;201(11):1459-67. doi: 10.1080/00986445.2013.818541
46. Yang H, Yan R, Chen H, Lee DH, Zheng C. Characteristics of hemicellulose, cellulose and lignin pyrolysis. Fuel. 2007 Aug;86(12-13):1781-8. doi: 10.1016/j.fuel.2006.12.013
47. Jung HY, Gupta RK, Oh EO, Kim YH, Whang CM. Vibrational spectroscopic studies of sol–gel derived physical and chemical bonded ORMOSILs. J Non-Cryst Solids. 2008 Mar;351(5):372-9. doi: 10.1016/j.jnoncrysol.2005.01.004
48. Sarangi M, Naya KP, Tiwari TN. Effect of temperature on nano-crystalline silica and carbon composites obtained from rice-husk ash. Compos. Part B Eng. 2011 Oct;42(7):1994-8. doi: 10.1016/j.compositesb.2011.05.026
49. Dey KP, Ghosh S, Naskar MK. Organic template-free synthesis of ZSM-5 zeolite particles using rice husk ash as silica source. Ceram Int. 2013 Mar;39(2):2153-7. doi: 10.1016/j.ceramint.2012.07.083
50. Fernandes IJ, Calheiro D, Kieling AG, Moraes CA, Rocha TL, Brehm FA, et al. Characterization of rice husk ash produced using different biomass combustion techniques for energy. Fuel. 2016 Feb;165:351-9. doi: 10.1016/j.fuel.2015.10.086
51. Hospodarova V, Singovszka E, Stevulova N. Characterization of cellulosic fibers by FTIR spectroscopy for their further implementation to building materials. Am J Anal Chem. 2018 Jun;9(6):303-10. doi: 10.4236/ajac.2018.96023
52. Fortunati E, Puglia D, Monti M, Peponi L, Santulli C, Kenny JM, et al. Extraction of cellulose nanocrystals from *Phormium tenax* fibres. J Polym Environ. 2013 Nov;21:319-28. doi: 10.1007/s10924-012-0543-1
53. Trajano HL, Wyman CE. Aqueous pretreatment of plant biomass for biological and chemical conversion to fuels and chemicals. In: Fundamentals of biomass pretreatment at low pH. Hoboken: Wiley; 2013. p. 103-28. doi: 10.1002/9780470975831.ch6
54. Irklei VM, Kleiner YY, Vavrinyuk OS, Gal'braikh LS. Kinetics of degradation of cellulose in basic medium. Fiber Chem. 2005 Nov;37(6):452-8. doi: 10.1007/s10692-006-0019-y
55. Hendriks ATWM, Zeeman G. Pretreatments to enhance the digestibility of lignocellulosic biomass. Bioresour Technol. 2009 Jan;100(1):10-8. doi: 10.1016/j.biortech.2008.05.027
56. Kulandaivel N, Muralikannan R, KalyanaSundaram S. Extraction and characterization of novel natural cellulosic fibers from pigeon pea plant. J Nat Fibers. 2018 Oct;17(5):1-11. doi: 10.1080/15440478.2018.1534184

57. Rao B, Dai H, Gao L, Xie H, Gao G, Peng K, et al. Surprisingly highly reactive silica that dissolves rapidly in dilute alkali (NaOH) solution even at ambient temperatures (25 °C). J Clean Prod. 2022;341:130779. doi: 10.1016/j.jclepro.2022.130779
58. Thommes M, Kaneko K, Neimark AV, Olivier JP, Rodriguez-Reinoso F, Rouquerol J, et al. Physisorption of gases, with special reference to the evaluation of surface area and pore size distribution (IUPAC Technical Report). Pure Appl. Chem. 2015 Jul;87(9-10):1051-69. doi: 10.1515/pac-2014-1117
59. Chen XG, Lv SS, Liu ST, Zhang PP, Zhang AB, Sun J, Ye Y. Adsorption of methylene blue by rice hull ash. Sep Sci Technol. 2012 Jan;47(1):147-56. doi: 10.1080/01496395.2011.606865
60. Wang L, Zhang J, Wang A. Removal of methylene blue from aqueous solution using chitosan-g-poly(acrylic acid)/montmorillonite superadsorbent nanocomposite. Colloids Surf. A Physicochem EngAspects. 2008 Jun;322(1-3):47-53. doi: 10.1016/j.colsurfa.2008.02.019
61. Mall ID, Srivastava VC, Kumar GVA, Mishra IM. Characterization and utilization of mesoporous fertilizer-plant-waste carbon for adsorptive removal of dyes from aqueous solution. Colloids Surf. A Physicochem. Eng. Aspects. 2006 Mar;278(1-3):175-87. doi: 10.1016/j.colsurfa.2005.12.017
62. Ahmad A, Khan N, Giri BS, Chowdhary P, Chaturvedi P. Removal of methylene blue dye using rice husk, cow dung, and sludge biochar: characterization, application, and kinetic studies. Bioresour Technol. 2020 Mar;306:123202. doi: 10.1016/j.biortech.2020.123202
63. Phihusut D, Chantharat M. Removal of methylene blue using agricultural waste: a case study of rice husk and rice husk ash from Chaipattana Rice Mill Demonstration Center. Environ Nat Resour J. 2017; 15(2):30-8 doi: 10.14456/ennrj.2017.10
64. Sharma A, Jain H, Miller AC. Surface modification of a silicate glass during XPS experiments. Surf Interface Anal. 2001 May;31(5):369-74.
65. Leung K, Nielsen IMB, Criscenti LJ. Elucidating the bimodal acid–base behavior of the water-silica interface from first principles. J Am Chem Soc. 2009 Dec;131(51):18358-65. doi: 10.1021/ja906190t
66. Foo KY, Hameed BH. Insights into the modeling of adsorption isotherm systems. Chem Eng J. 2010 Jan;156(1):2-10. doi: 10.1016/j.cej.2009.09.013
67. Bertolani AG, da Silva CH, da Silva Andrade JG, Scaliante MHNO, Rosa SLF, et al. Hydrocarbonization of the pigeon pea husk as an alternative to increase the biosorption of the industrial dye yellow tartrazine from aqueous solutions. Braz J Anim Environ Res. 2024;7(4):e74218. doi: 10.34188/bjaerv7n4-037
68. Hongo T, Moriura M, Hatada Y, Abiko H. Simultaneous methylene blue adsorption and pH neutralization of contaminated water by rice husk ash. ACS Omega. 2021 Aug;6(33):21604-12. doi: 10.1021/acsomega.1c02734
69. Piccin JS, Cadaval TRSA, de Pinto LAA, Dotto GL. Adsorption isotherms in liquid phase: experimental, modeling, and interpretations. In: Adsorption processes for water treatment and purification. Cham: Springer; 2017. p. 19-51. doi: 10.1007/978-3-319-58136-1_2
70. Salem IA, Fayed TA, El-Nahass MN, Dawood M. A comparative study for adsorption of methylene blue dye from wastewater onto three different types of rice ash. J Pharm Appl Chem. 2018;4(2):30-9.
71. De Araújo TP, Tavares FDO, Vareschini DT, Barros MAS. Biosorption mechanisms of cationic and anionic dyes in a low-cost residue from brewer's spent grain. Environ Technol. 2021 Jan;42(19):2925-40. doi: 10.1080/09593330.2020.1718217
72. Nascimento RF, Lima ACA, Vidal CB, Melo DDQ, Raulino GSC. Adsorção*:* aspectos teóricos e aplicações ambientais. 2. ed. Fortaleza (SE): Imprensa Universitária; 2020.